Ion trapping, reduced rotational viscosity, and accelerated electro-optic response characteristics in gold nano-urchin–nematic suspensions

Rajratan Basu ●* and Derek T. Gess ●

Department of Physics, Soft Matter and Nanomaterials Laboratory,
The United States Naval Academy, Annapolis, Maryland 21402, USA

The free-ion concentration in a nematic liquid crystal (LC) is found to be significantly reduced when gold nano-urchins (AuNUs) of 50-nm diameter are dispersed in the LC in dilute concentrations. The nano-urchins on AuNUs trap a significant amount of mobile ions, reducing the free-ion concentration in the LC media. The reduction of free ions results in a decreased rotational viscosity and accelerated electro-optic response of the LC. The study is carried out with several AuNUs concentrations in the LC, and the experimental results consistently suggest that there exists an optimal concentration of AuNUs, above which they tend to aggregate. At the optimal concentration, the ion trapping is maximum, rotational viscosity is at its lowest, and the electro-optic response is the fastest. Above this optimal AuNUs concentration, the rotational viscosity is found to increase, and consequently, the LC no longer exhibits an accelerated electro-optic response.

I. INTRODUCTION

The presence of excess ionic impurities [1,2] in liquid crystals (LC) triggers complications in electro-optical liquid-crystal displays (LCDs). The ion-related issues in LCDs include slow responses, short-term flickering, and long-term image-sticking effects [3–9]. These free ions generally originate from the LC's chemical synthesis process, the LC cell's conductive electrodes [10,11], and the polyimide (PI) alignment layers [12]. Chemical decomposition and self-dissociation of the LC materials can also introduce ionic contamination [13]. Therefore, investigating the influence of the free ions on the LC's electrical, mechanical, and electro-optical properties [14–21] is an important area of fundamental and applied research.

There are existing methods to reduce ionic contamination in the LC. For example, the ion impurities can be reduced by employing extremely purified reagents during the chemical synthesis of the LCs [22]. Traditional methods, such as chromatography, zone refining, multiple recrystallizations, vacuum distillation, extraction, vacuum sublimation, ion exchange, and electrodialysis [22–26] are also utilized to reduce the excess ionic impurities. However, these techniques of purifying LCs from ionic impurities are expensive, lengthy, and labor consuming [22]. Additionally, highly purified LCs can again get ionic impurities during the time of device fabrication from the cell's electrodes, PI alignment layers, and glue [10–12]. Therefore, developing new approaches to purifying the LCs from ionic impurities is essential.

Over the last decade, an exciting research direction has been an attempt to reduce the free-ion concentration by exploiting various nanomaterials instead of the extensive chemical process. Recent reports show that the colloidal dispersion of nanomaterials, such as ferroelectric nanoparticles [27,28], titanium nanoparticles [29], carbon nanotubes [30–32], graphene [33–37], and fullerenes [36,38,39] in the LC can suppress the free-ion concentration by the ion-trapping process. Two-dimensional alignment layers, such as graphene and hexagonal boron nitride, can also capture free ions from the LC [40,41]. The ion-capturing process by doping nanomaterials in the LC can enhance the overall performance of LC-based electro-optic devices [35,42].

Gold nano-urchins (AuNUs) [43], also termed gold nanoflowers or gold nanostars, are novel multibranched nanoparticles. The spikelike nano-urchins on the gold nanoparticle surface are the basis for unique optical features that can be exploited for basic research, sensor development, and other applications [44]. This paper presents that a small quantity of AuNUs in the LC traps a significant amount (~60%) of free ions. The ions get trapped at the anisotropic spikelike outer surface of the AuNUs. Figure 1(a) schematically shows the presence of ions in a nematic phase. Figure 1(b) schematically shows the ion-trapping phenomenon by the AuNUs in the LC. Figure 1(c) is a scanning electron microscopy (SEM) image of a AuNU particle. Our experiments reveal that the significant reduction of the ionic impurities alters the LC's intrinsic properties, such as rotational viscosity, dielectric anisotropy, and dynamic electro-optic response times. We also show that the concentration of the AuNUs has a crucial role in altering these intrinsic properties. Above a specific concentration of the AuNUs—which we call an optimal concentration—these LC properties still change, but in the opposite direction.

II. EXPERIMENTS, RESULTS, AND DISCUSSIONS

A. Ion concentration

Nonfunctionalized AuNUs of 50-nm diameter in ethanol solvent were obtained from NNCrystal US Corporation. The
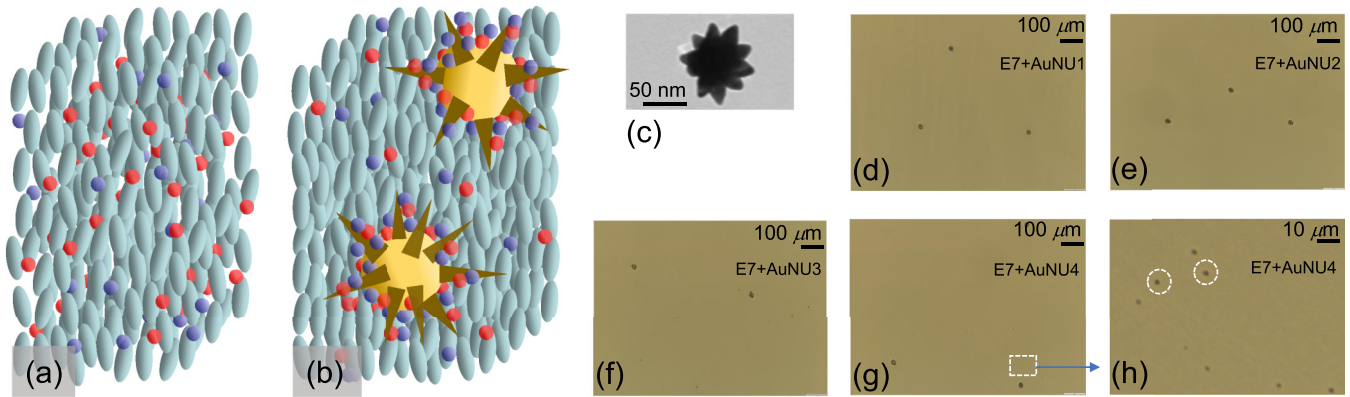
---

*basu@usna.edu

024705-1

FIG. 1. Schematic illustration of the presence of ions and AuNUs in the nematic phase. Small spheres represent the ions, the ellipsoids represent LC molecules, and the big spheres with spikes represent the AuNUs. (a) Random distribution of free ions in a nematic phase. (b) AuNUs' ion-trapping process in a nematic phase. (c) SEM image of a AuNU particle. Optical microphotographs under a cross-polarized microscope for (d) E7+AuNU1, (e) E7+AuNU2, (f) E7+AuNU3, and (g) E7+AuNU4 samples. The 20-μm spacer particles from the LC cells are visible, and no graphene aggregates are observed for E7+AuNU1 and E7+AuNU2. In addition to the spacer particles, several small aggregates are observed as small dark spots for E7+AuNU3 and E7+AuNU4. (h) A 10× magnified image of the dashed rectangular region of (g). Two such AuNU aggregates are shown in two dashed circles. Scale bar is shown in each microphotograph.

ethanol+AuNUs solution was first remixed by sonication for 2 h. The liquid crystal E7 (EMD Millipore Corporation, $T_{NI} = 60.0\,°C$) then was added to the ethanol+AuNUs and sonicated for 2 h. This allowed the LC to dissolve into the solution. The ethanol solvent was then evaporated slowly at an elevated temperature, leaving a pure LC+AuNUs mixture. Finally, the LC+AuNUs was degassed under a vacuum for 5 h. This method was repeated to produce four known concentrations of AuNUs in the LC : E7 + AuNU1 = 7.26×10^{-4} wt. %, E7 + AuNU2 = 13.4×10^{-4} wt. %, E7 + AuNU3 = 24.8×10^{-4} wt. %, and E7 + AuNU4 = 35.2×10^{-4} wt. %. For uniformity, the pure LC E7 was also treated the same way, such as dissolving in ethanol followed by slow evaporation and degassing. Commercially manufactured planar LC test cells (SA100A200uG180) from Instec, Inc., with 1-cm^2 indium-tin-oxide–coated area, a $d = 20$-μm spacing, and a $1.5°$ pretilt angle were used for our studies. The test cells were filled by capillary action with the pure E7 or the E7+AuNU mixtures at temperature $T > 65\,°C$ in the isotropic phase and slowly cooled to room temperature. Before performing any experiments, the test cells were examined using a cross-polarized microscope. Figures 1(d), 1(e), 1(f), and 1(g) show the micrographs of E7+AuNU1, E7+AuNU2, E7+AuNU3, and E7+AuNU4, respectively. Figure 1(h) presents a 10× magnified version of the dashed square in Fig. 1(g). A detailed explanation of these micrographs is discussed later.

The free-ion concentration, n_i, in LC E7 and E7+AuNU mixtures was measured from the transient ion current, I_{ion}, generated by inverting the polarity of the applied voltage across the cell [28,45]. When a square-wave voltage changing from $+V$ to $-V$ (i.e., the voltage polarity is inverted) is applied across the cell, the LC molecules do not rotate as the director rotation depends only on the *magnitude* of the electric field E, and not on its *polarity* [46]. However, inverting the voltage polarity triggers the motion of the ions in the LC towards the opposite electrodes—which results in a transient ion current, I_{ion}, in the cell. A square-wave

peak-to-peak voltage of 20 V (i.e., +10 to −10 V) at 1 Hz was applied using an Automatic Liquid Crystal Tester (Instec, Inc.) to generate I_{ion} as a function of time in the test cells, as shown in Fig. 2(a) at $T = 35\,°C$. We performed this measurement for all five samples but presented the I_{ion} only for the first three samples in Fig. 2(a) to keep the graph less crowded. Note that I_{ion} reaches its peak value when the positive and negative ions meet approximately at the middle of the cell. The peak time is defined by $t_{ion\,peak} = \frac{d^2}{2\mu E}$, where μ is the mobility [45]. Finally, I_{ion} decays to zero when the positive and negative ions reach the opposite electrodes—which can be seen in Fig. 2(a). The total free-ion transport in the test cells was then calculated by taking the area under the I_{ion} vs time curve. The free-ion concentration, $n_i = (\int_0^t I_{ion} dt)/Ad$, was extracted using the known cell-gap d and active area A of the cell. At higher temperatures, there are more ions, and the mobility of ions is larger. Figure 2(b) presents n_i for all five samples as a function of temperature, depicting that n_i is substantially suppressed for E7+AuNU1 and E7+AuNU2 compared to pure E7. Note that n_i is suppressed by ~60% at the middle of the temperature range (45 °C) for the AuNU2 sample. Interestingly, n_i for E7+AuNU3 and E7+AuNU4 no longer decreases any further. In fact, n_i for E7+AuNU3 is higher than E7+AuNU1 and E7+AuNU2, but stays lower than pure E7. And, n_i for E7+AuNU4 is very similar to that of the pure E7, indicating that this mixture does not effectively trap ions anymore. We will address this issue later from the AuNU-aggregation viewpoint. Note that there is no known attractive force between the AuNUs and the free ions. The free ions get trapped on the AuNUs because of the presence of asymmetric spikelike nano-urchins on the gold nanoparticle surface. We therefore expect the AuNUs to trap both the positive and negative ions equally in the LC.

It is important to compare the ion-trapping ability of AuNUs with other nanomaterials. It was reported that 0.5 wt. % of graphene nanoplatelets in LC 8OCB led to a 30% reduction in ion concentration [22]. An approximately
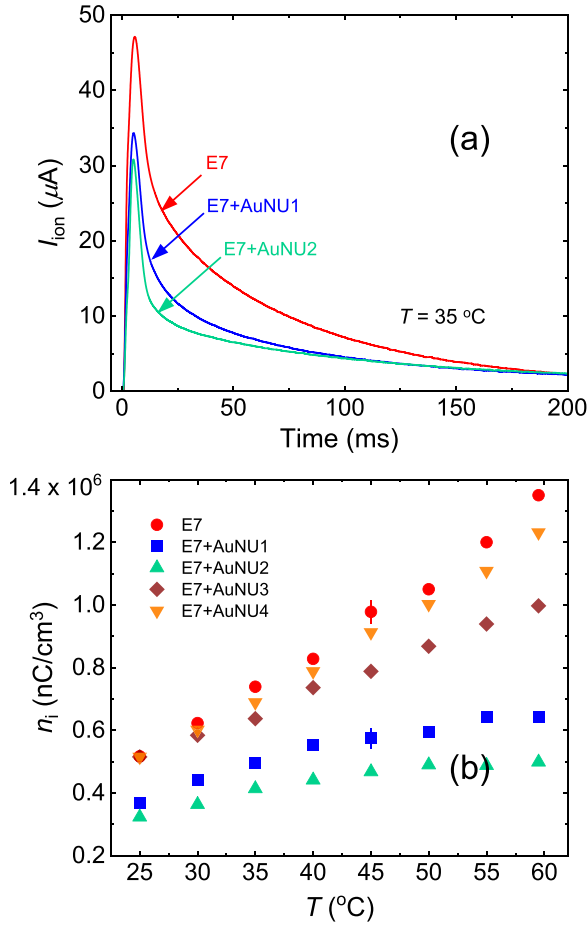
FIG. 2. (a) Ion current, I_{ion}, as a function of time for E7, E7+AuNU1, and E7+AuNU2 at $35\,°C$ after the voltage is inverted across the cells. The peak represents the ion bump when positive and negative ions meet in the middle of the cell. (b) Free-ion concentration, n_i, as a function of temperature for E7 and four different E7+AuNU samples listed in the legend. Typical error bars are shown.

32% reduction in ion concentration was reported by 0.5 wt. % graphene platelets in cholesteric LCs [22]. Almost 80% ion reduction was found when a ferroelectric LC was doped with 0.5 wt. % of fullerenes, C_{60}. Ferroelectric nanoparticles ($BaTiO_3$), at 0.275 w%, in LC 5CB were found to trap 50% of the free ions [28]. In another study [22], titanium dioxide (TiO_2) nanoparticles (0.1 w%) were found to absorb 53% ion impurities in LC E7. In our experiments, we used AuNUs at $\sim 10^{-3}$ wt. % concentration in E7 (for the E7+AuNU2 sample), and they trapped $\sim 60\%$ free ions in the LC. So, the ion-trapping ability of AuNUs is in a similar range to the other nanoparticles reported earlier. However, AuNUs trap ions at much lower doping concentrations than other nanoparticles.

B. Rotational viscosity

Rotational viscosity, γ_1, of an aligned LC, represents internal friction among LC molecules during the rotation process. We performed experiments to study γ_1 of the LC samples. The rotational viscosity for the nematic samples was obtained by measuring the transient current induced by a DC field across
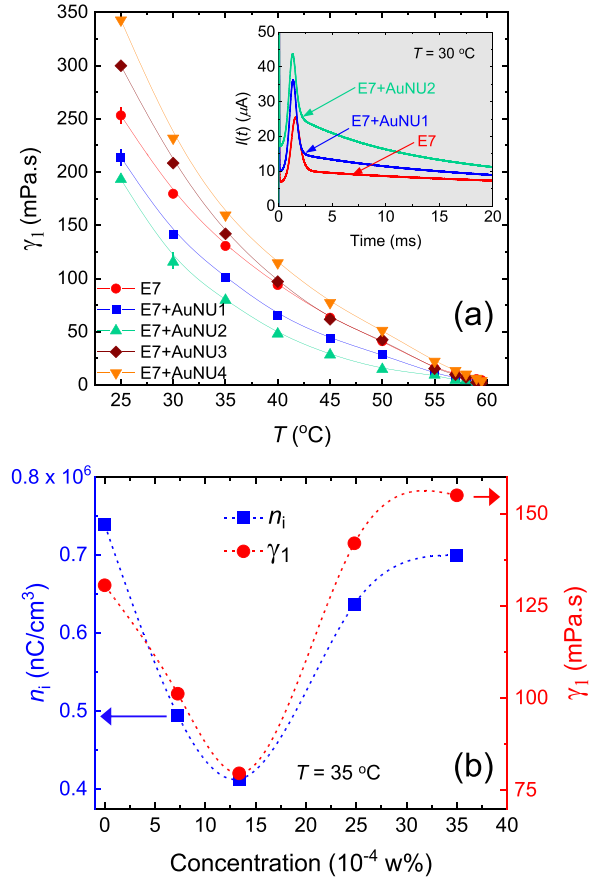

FIG. 3. (a) Rotational viscosity, γ_1, as a function of temperature for E7 and four E7+AuNU samples, listed in the legend. Inset: Transient current, $I(t)$, as a function of time for E7, E7+AuNU1, and E7+AuNU2 at $T = 30\,°C$. Typical error bars are shown. (b) γ_1 (right-Y axis) and n_i (left-Y axis) as a function of AuNU concentration at $T = 35\,°C$. Dotted lines are a guide to the eye.

a planar-aligned capacitive-type cell configuration [47–49]. When a DC field (much higher than the threshold field) is applied across a planar LC cell, the induced current $I(t)$ through the cell shows a time response as the nematic director goes through the dynamic rotation. The current response is given by

$$I(t) = \frac{A\,(\Delta\varepsilon\,\varepsilon_o)^2\,E^3}{\gamma_1}\sin^2[2\theta(t)], \qquad (1)$$

where A is the area of the cell, E is the electric field, and θ is the angle the director makes with the electrodes at a given time. At $\theta = 45°$, $I(t)$ reaches its peak, $I_p = \frac{A\,(\Delta\varepsilon\,\varepsilon_o)^2\,E^3}{\gamma_1}$ at the peak time,

$$t_p = \left[\frac{\gamma_1[-\ln(\tan\theta_o)]}{\Delta\varepsilon\,\varepsilon_o}\right]\frac{1}{E^2}, \qquad (2)$$

where θ_o is the pretilt angle. A DC field pulse with a pulse interval of 1 Hz was applied across the cell to generate $I(t)$. Then, $I(t)$ in the cell was detected as a function of time through a load resistor in series by a digital storage oscilloscope. The inset in Fig. 3(a) shows an example of $I(t)$ as a function of time for three different test cells, E7, E7+AuNU1, and AuNU2, at

$T = 30\,^\circ\text{C}$. The peak current, I_p, was detected from the $I(t)$ vs time graph to extract γ_1 from the known values of E, $\Delta\varepsilon$, and A. The measurement of $\Delta\varepsilon$ is discussed later. Figure 3(a) represents γ_1 as a function of temperature for the test cells listed in the legend. γ_1 shows the pretransitional behavior for all the samples. Clearly, E7+AuNU1 and E7+AuNU2 exhibit a significant decrease in γ_1 compared to pure E7. In the temperature range from $25\,^\circ\text{C}$ to $45\,^\circ\text{C}$, the average reduction in γ_1 for E7+AuNU2 is $\sim 30\%$.

There have been reports in the literature that suggest that the rotational viscosity of an LC decreases due to the suppression of ionic impurities. For example, a recent report [50] shows that the presence of quantum dots in an LC can suppress the ionic impurities—which causes a reduction in the overall ionic density and the resistance of the nematic medium. Consequently, the rotational viscosity of the quantum dot-doped LC system is reduced. Our group previously found [33] that graphene flakes can trap ionic impurities in a ferroelectric LC and reduce rotational viscosity. Another report in the literature [29] shows that Ti nanoparticles trap ions, leading to stronger van der Waals dispersion interactions between LC molecules and the alignment layers—which results in a smaller pretilt angle of the LC molecules at the alignment layers. From Eq. (2), $\gamma_1 \propto 1/[-\ln(\tan\theta_\text{o})]$, where θ_o is the pretilt angle. This equation suggests that when θ_o decreases, γ_1 also decreases. We believe that due to the reduction of ionic impurities in the E7+AuNU1 and E7+AuNU2 samples, the internal resistance (friction) is reduced, and the van der Waals dispersion interactions between LC molecules and the alignment layers are enhanced (hence a decrease in the pretilt angle). Thus, γ_1 is reduced in the two samples.

No quantitative theoretical model yet directly relates the ion concentrations to γ_1. However, we believe that reports in the literature mentioned above coherently suggest that the decrease in ionic impurities in the LC decreases γ_1, which is consistent with our results presented here.

Figures 2(b) and 3(a) show that n_i and γ_1, respectively, decrease for E7+AuNU1 and E7+AuNU2 and then increase for E7+AuNU3 and E7+AuNU4. This indicates that the E7+AuNU2 sample is the best or the most favorable concentration as far as the maximum decrease in n_i and γ_1 is concerned. We call this concentration the *optimal concentration*. Figure 3(b) shows γ_1 (right-Y axis) and n_i (left-Y axis) as a function of AuNU concentration at $T = 35\,^\circ\text{C}$, depicting a clear correlation between n_i and γ_1. This correlation indicates that a decrease in n_i results in a reduction of γ_1. Also, note that two independent measurements, i.e., n_i and γ_1, indicate the same optimal AuNU concentration—E7+AuNU2.

The presence of the optimal concentration may be explained from the AuNUs aggregation viewpoint. As mentioned before, pure E7 and E7+AuNU samples were examined under a transmitted cross-polarized microscope. Pure E7, as expected, revealed a uniform nematic texture. Similarly, E7+AuNU1 and E7+AuNU2 exhibited uniform nematic textures, with no indication of phase separation or agglomerates of AuNUs at any temperature. See the micrographs in Figs. 1(d) and 1(e). Only 20-μm spacer particles are visible in the micrographs. AuNUs start to aggregate when their concentration increases above E7+AuNU2 (i.e., above the optimal concentration) in the LC. Figures 1(f) and 1(g) show the
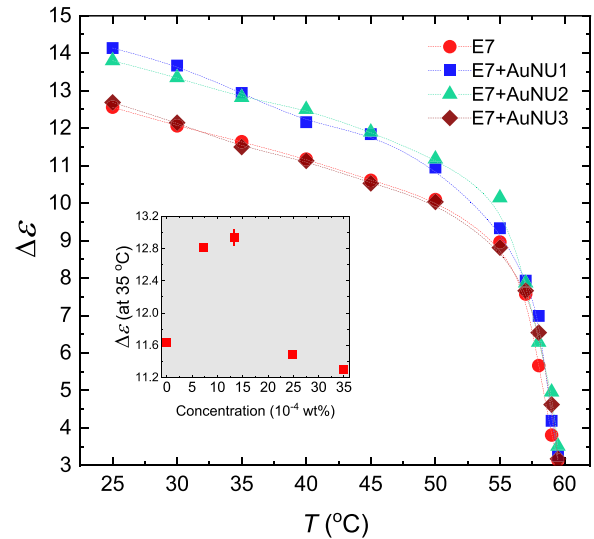

FIG. 4. Dielectric anisotropy, $\Delta\varepsilon$, as a function of temperature for E7 and E7+AuNU samples, listed in the legend. Inset: Dielectric anisotropy, $\Delta\varepsilon$, as a function of AuNU concentration at $T = 35\,^\circ\text{C}$. Typical error bars are shown.

microphotographs of E7+AuNU3 and E7+AuNU4 samples, respectively. A careful examination reveals that many small black dots are visible in addition to the 20-μm spacer particles in those micrographs. The white square region in Fig. 1(g) is magnified $10\times$ in Fig. 1(h), clearly showing several dark spots in E7+AuNU4. These dark spots are much smaller than the 20-μm spacer particles. We identify these dark spots as AuNU aggregates. Two such dark spots are highlighted using dashed circles in Fig. 1(h).

The AuNUs in aggregated form would not effectively suspend in the LC molecules and tend to phase separate. Therefore, the aggregated AuNUs would not be effective in capturing ions. The AuNUs at high concentrations and in aggregated form in the LC media introduce some degree of internal friction, preventing us from getting the best out of the ion-trapping process. In other words, large aggregates can act as *external additives* and most likely increase the internal friction of the LC. We therefore believe that γ_1 starts to increase due to AuNU aggregation above the optimal concentration. For similar reasons, the changes in $\Delta\varepsilon$ are also observed.

C. Dielectric anisotropy

The nematic phase shows dielectric anisotropy, $\Delta\varepsilon = \varepsilon_\parallel - \varepsilon_\perp$, where $\varepsilon_\parallel$ and $\varepsilon_\perp$ are the dielectric components parallel and perpendicular to the nematic director, respectively. An Automatic Liquid Crystal Tester (Instec, Inc.) was used to measure the dielectric constant ε as a function of the electric field at 1000 Hz for E7 and E7+AuNU samples. Then, $\Delta\varepsilon$ was obtained from $\varepsilon_\parallel$ and $\varepsilon_\perp$ (the detail is given elsewhere [51]). Figure 4 demonstrates the temperature dependence of $\Delta\varepsilon$ for E7 and E7+AuNU samples. The inset in Fig. 4 shows $\Delta\varepsilon$ as a function of AuNU concentration at $T = 35\,^\circ\text{C}$. Clearly, $\Delta\varepsilon$ increases monotonically for E7+AuNU1 and E7+AuNU2, and then it starts to decrease for E7+AuNU3 and E7+AuNU4. The result shown in the inset in Fig. 4 also independently ex-

hibits the presence of the *optimal concentration*, E7+AuNU2, for the enhancement in $\Delta\varepsilon$.

According to Maier and Meier's theory, the dielectric anisotropy $\Delta\varepsilon$ in the nematic phase is given by [52]

$$\Delta\varepsilon = \frac{NhFS}{\varepsilon_0}\left[\Delta\alpha + \frac{\mu^2 F}{2k_B T}(3\cos^2\beta - 1)\right]. \quad (3)$$

Here N is the number density, μ is the resultant dipole moment, $\Delta\alpha$ polarizability anisotropy, S is the order parameter, β is the angle between the long molecular axis and dipole moment of LC molecules, h is the cavity field factor, and F is the feedback factor [52].

When excess ionic impurities are present in the LC, it is possible that some negative ions accumulate on the positive side and some positive ions accumulate on the negative side of the LC molecules since an LC molecule has a permanent dipole moment. This ion accumulation reduces the

effective polarity of the LC molecules, resulting in a decrease in the effective value of μ. A reduction in μ results in a decrease in $\Delta\varepsilon$, according to Eq. (3). We, therefore believe that when the ionic impurities are suppressed in E7+AuNU1 and E7+AuNU2, the effective polarity of the LC molecules is improved, and we observe a higher $\Delta\varepsilon$. A report in the literature [53] shows that $\Delta\varepsilon$ of a nematic LC increases when TiO_2 nanoparticles are doped (at 0.2 wt. %) in the LC, and the authors attribute that to the ion-trapping process by the TiO_2 nanoparticles. Another report in the literature [50] shows that quantum dots (at 0.05 wt. %) can capture ions in a nematic LC, and the LC's birefringence is enhanced. This also suggests that when ionic impurities are suppressed, the LC's orientational order parameter S increases; thus, an increase in $\Delta\varepsilon$ is observed.

The number density of the free ions in the LC E7 is $\sim10^{16}/cm^3$ [from Fig. 2(b)]. The number density of the doped
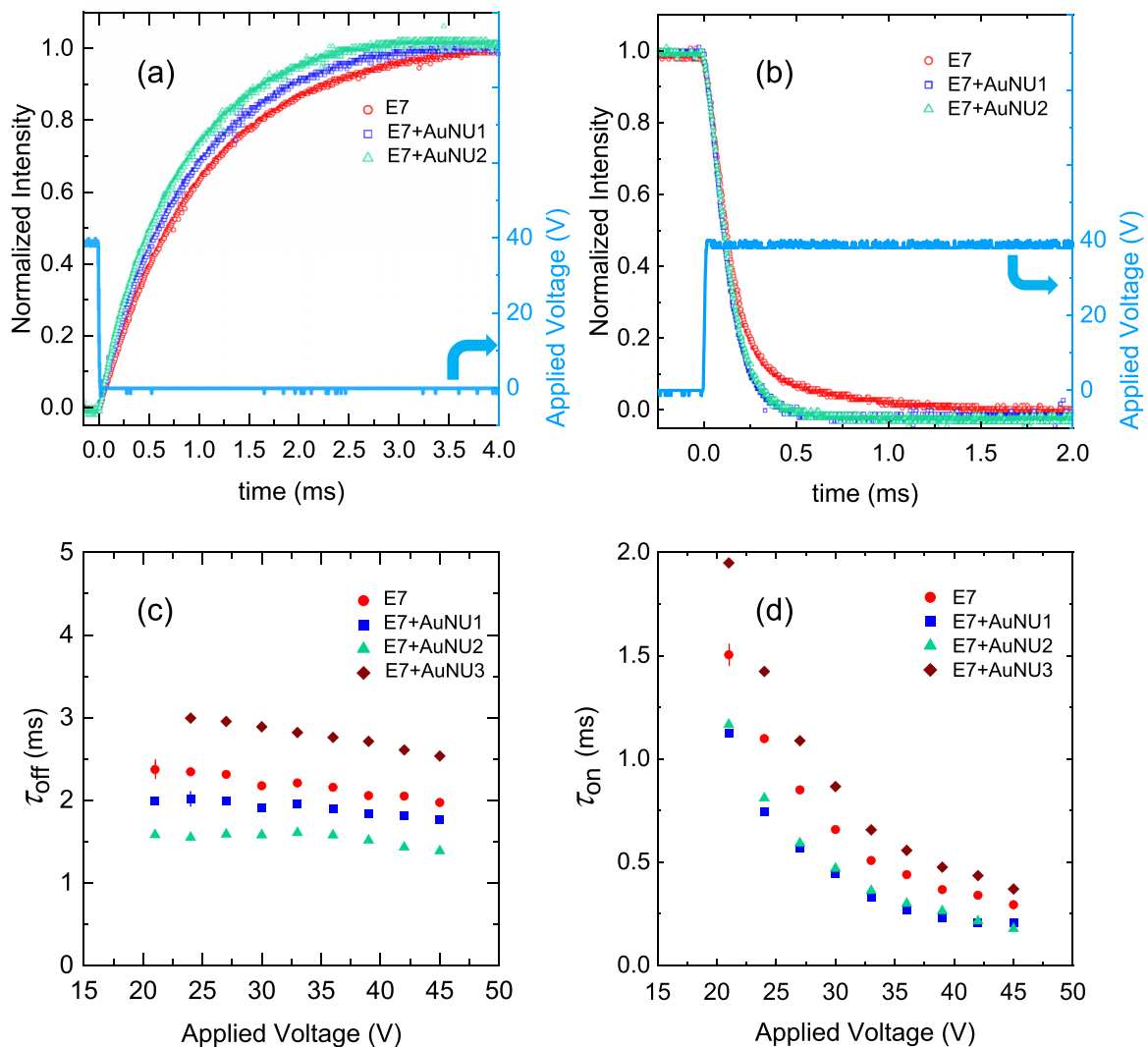

FIG. 5. Dynamic electro-optic switching of E7 and E7+AuNU samples. (a) The left-Y axis shows the normalized transmitted intensity as a function of time when a 40-V applied voltage is turned off, for the test cells listed in the legend ($T = 20\,°C$). The right-Y axis shows the applied voltage profile. (b) Left-Y axis shows the normalized transmitted intensity as a function of time when a 40-V applied voltage is turned on, for the test cells listed in the legend ($T = 20\,°C$). The right-Y axis shows the applied voltage profile. (c) Optical switching off, τ_{off}, and (d) optical switching on, τ_{on}, as a function of applied voltage for E7 and E7+AuNU samples listed in the legend. Typical error bars are shown.

AuNUs in the LC is $\sim 10^9/\text{cm}^3$ (determined from a AuNU particle mass, $m_{\text{AuNU}} = 1.27 \times 10^{-15}$ g). Also, the ions are much smaller in size than the AuNUs. Thus, the ions can effectively accumulate around the LC molecules due to their large number density and smaller size and, then, can affect the polarity of the LC molecules. The AuNUs, on the other hand, cannot affect the polarity of the LC molecules since the AuNUs are neutral. Therefore, the AuNUs, in nonaggregated forms, do not change the LC characteristics significantly.

At higher concentrations (E7+AuNU3 and E7+AuNU4), when AuNUs aggregate in the LC, they no longer effectively trap ions. Therefore, $\Delta\varepsilon$ does not increase any further for these two higher concentrations. In aggregated forms (E7+AuNU3 and E7+AuNU4), we believe the AuNUs distort the nematic director field locally, and the overall orientational order decreases slightly. Consequently, the order parameter S also decreases. The dielectric anisotropy $\Delta\varepsilon$ is proportional to S, according to Eq. (3). Therefore, we observe a slight decrease in $\Delta\varepsilon$ for E7+AuNU3 and E7+AuNU4.

D. Electro-optic effect

The rotational viscosity, γ_1, is linearly proportional to the dynamic electro-optic response of an aligned nematic LC. Since γ_1 is significantly altered for the E7+AuNU samples, we have studied the dynamic electro-optic response of these hybrid samples and compared that with the pure E7. The dynamic electro-optic response was studied using an optical setup with a 5-mW He-Ne laser beam ($\lambda = 633$ nm) sent through a polarizer, the LC cell (where the director was oriented at 45° with respect to the polarizer), a crossed analyzer, and into a photodetector. The output of the photodetector was connected to a digital storage oscilloscope to detect the change in the transmitted intensity through the cell as a function of time when a square-wave voltage of 30 Hz was applied across the cell. Transmittance responses were studied for several applied voltages much higher than the orientation threshold switching voltage, V_{th}, at $T = 20$ °C. In Fig. 5(a), the left-y axis represents the normalized transmitted intensity of LC E7, E7+AuNU1, and E7+AuNU2 as a function of time when a square-wave voltage (40 V) was turned off. Similarly, in Fig. 5(b), the left-y axis represents the normalized transmitted intensity of the same three samples as a function of time when the square-wave voltage (40 V) was turned on. After the voltage is turned on, the transmitted intensity through the cell decreases. The time it takes to drop from 90 to 10% of its maximum value is defined as the optical switching on, τ_{on}. After the voltage is turned off, the transmitted intensity increases, and the optical switching off, τ_{off}, is defined by the time it takes to rise from 10 to 90% of its maximum value. These two switching times, τ_{on} and τ_{off}, are described as [54]

$$\tau_{\text{on}} \propto \frac{\gamma_1 \, d^2}{\Delta\varepsilon \, \varepsilon_o \, V^2 - K_{11} \, \pi^2}; \quad \tau_{\text{off}} \propto \frac{\gamma_1 \, d^2}{K_{11} \, \pi^2}, \quad (4)$$

where γ_1 is the rotational viscosity, d is the cell gap, $\Delta\varepsilon$ is the dielectric anisotropy, V is the applied voltage, ε_0 the is free-space permittivity, and K_{11} is the splay elastic constant.

Figures 5(c) and 5(d) show τ_{off} and τ_{on}, respectively, for the samples as a function of applied voltage, V. Clearly, τ_{off} and τ_{on} are both faster for E7+AuNU1 and E7+AuNU2 compared

to that of the pure E7. Note that the switching off, τ_{off}, is $\sim 35\%$ faster, and the switching on, τ_{on}, is $\sim 33\%$ faster for the E7+AuNU2 sample compared to the pure E7. A reduction of free ions lessens γ_1 in those two samples—which governs this faster response. At the higher concentrations, γ_1 is increased due to the AuNU aggregations; therefore, the electro-optic switching is slower. The dynamic response of the E7+AuNU3 sample is not shown in Figs. 5(a) and 5(b) to keep the figures less crowded. Only τ_{off} and τ_{on} for this concentration are shown in Figs. 5(c) and 5(d) for proper comparison. Since the response times for the E7+AuNU3 sample are already higher than the pure E7, we did not conduct this dynamic electro-optic study for the E7+AuNU4 sample, knowing that it will also show a slower response.

E. Robustness of AuNUs for ion trapping

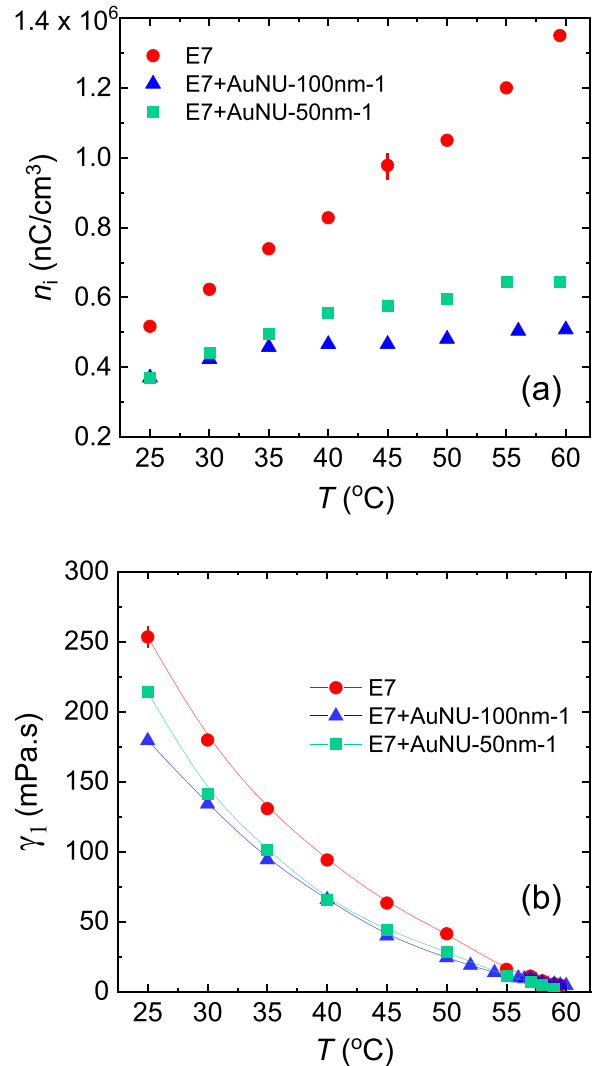To understand the robustness of the ion-trapping capabilities of AuNUs, we next chose a different diameter

FIG. 6. (a) Free-ion concentration, n_i, as a function of temperature for E7 and two E7+AuNU samples of different sizes (100 and 50 nm), as listed in the legend. (b) Rotational viscosity, γ_1, as a function of temperature for E7 and two E7+AuNU samples of different sizes (100 and 50 nm), as listed in the legend. Typical error bars are shown.

(100 nm) of these nanoparticles and repeated the ion measurement study. At the lowest concentration, 7.26×10^{-4} wt. % (E7+AuNU-100 nm-1), we observed a similar ion-trapping trend compared to the 50-nm concentration. See Fig. 6(a). We also measured the rotational viscosity for E7+AuNU-100 nm-1. Similar to the previous E7+AuNU 1, the new E7+AuNU-100 nm-1 also showed a decrease in γ_1. These results suggest that the AuNUs from different batches (50 and 100 nm) can effectively trap ions and lower the γ_1. We did not conduct any concentration-dependent study for the 100-nm AuNUs. The only purpose of using the 100-nm AuNUs was to test whether the ion trapping was reproducible with another batch of AuNUPs. Thus, the results are not artifacts but actual ion-trapping phenomena.

III. CONCLUSION

We have experimentally demonstrated that a small quantity of AuNUs in the LC can lower the LC's free-ion concentration by the ion-trapping process. Our AuNU concentration-dependent study indicates that there exists an optimal concentration of AuNUs, above which the ion trapping by the dispersed AuNUs is not significant. Below or at the optimal concentration (E7+AuNU1 and E7+AuNU2), where the ion trapping by the dispersed AuNUs is more effective, the presence of the free ions is significantly suppressed. The presence of fewer mobile ions decreases the internal friction of the nematic media, enabling the nematic director to rotate faster.

Therefore, the rotational viscosity was observed to decrease below the optimal concentration. However, being embedded in the LC, the AuNUs themselves act as external additives and can increase the internal friction in the LC. Therefore, in one way, the reduction of free ions tends to decrease the rotational viscosity, and in the other way, higher AuNU concentrations tend to increase the rotational viscosity. When the concentration of AuNUs increases above a specific limit (optimal concentration), they tend to aggregate and rapidly enhance the internal friction of the LC. The presence of AuNUs at higher concentrations (E7+AuNU3 and E7+AuNU4) overmatches the impact of the reduction of ions on the rotational viscosity. Consequently, the rotational viscosity was observed to increase above the optimal concentration. We have also experimentally shown that the decrease of free ions and the lower rotational viscosity, below the optimal concentration, resulted in an accelerated electro-optic response of the LC. We repeated the experiments with a different size of AuNUs and observed a similar result of ion reduction. This proves that the AuNUs are also effective in trapping ions at different sizes. These results are important for purifying LCs from excess ionic impurities, and concentration-dependent study reveals a scientifically intriguing feature of the existence of an optimal concentration.

[1] G. H. Heilmeier and P. M. Heyman, Note on Transient Current Measurements in Liquid Crystals and Related Systems, Phys. Rev. Lett. **18**, 583 (1967).

[2] G. Briere, F. Gaspard, and R. Herino, Ionic residual conduction in the isotropic phase of a nematic liquid crystal, Chem. Phys. Lett. **9**, 285 (1971).

[3] S. Takahashi, The investigation of a dc induced transient optical 30-Hz element in twisted nematic liquid-crystal displays, J. Appl. Phys. **70**, 5346 (1991).

[4] H. De Vleeschouwer, B. Verweire, K. D'Have, and H. Zhang, Electrical and optical measurements of the image sticking effect in nematic LCD's, Mol. Cryst. Liq. Cryst. **331**, 567 (1999).

[5] H. De Vleeschouwer, F. Bougrioua, and H. Pauwels, Importance of ion transport in industrial LCD applications, Mol. Cryst. Liq. Cryst. **360**, 29 (2001).

[6] D. Xu, F. Peng, H. Chen, J. Yuan, S.-T. Wu, M.-C. Li, S.-L. Lee, and W.-C. Tsai, Image sticking in liquid crystal displays with lateral electric fields, J. Appl. Phys. **116**, 193102 (2014).

[7] H. De Vleeschouwer, A. Verschueren, F. Bougrioua, R. van Asselt, E. Alexander, S. Vermael, K. Neyts, and H. Pauwels, Long-term ion transport in nematic liquid crystal displays, Jpn. J. Appl. Phys. **40**, 3272 (2001).

[8] K. H. Yang, Charge retention of twisted nematic liquid-crystal displays, J. Appl. Phys. **67**, 36 (1990).

[9] N. Sasaki, A new measurement method for ion density in TFT-LCD panels, Mol. Cryst. Liq. Cryst. **367**, 671 (2001).

[10] S. Murakami and H. Naito, Charge injection and generation in nematic liquid crystal cells, Jpn. J. Appl. Phys. **36**, 773 (1997).

[11] S. Naemura and A. Sawada, Ion generation in liquid crystals under electric field, Mol. Cryst. Liq. Cryst. **346**, 155 (2000).

[12] N. A. J. M. Van Aerle, Influence of polyimide orientation layer material on the liquid crystal resistivity in LCDs, Mol. Cryst. Liq. Cryst. **257**, 193 (1994).

[13] M. Sierakowski, Ionic interface-effects in electro-optical LC-cells, Mol. Cryst. Liquid Cryst. **375**, 659 (2002).

[14] K. Neyts, S. Vermael, C. Desimpel, G. Stojmenovik, R. van Asselt, A. R. M. Verschueren, D. K. G. de Boer, R. Snijkers, P. Machiels, and A. van Brandenburg, Lateral ion transport in nematic liquid-crystal devices, J. Appl. Phys. **94**, 3891 (2003).

[15] M. Yamashita and Y. Amemiya, Drift mobility of positive ions in nematic MBBA at low electric field, Jpn. J. Appl. Phys. **17**, 1513 (1978).

[16] V. Novotny, Measurement of mobilities of particles in liquids by optical and electrical transients, J. Appl. Phys. **50**, 2787 (1979).

[17] A. Sugimura, N. Matsui, Y. Takahashi, H. Sonomura, H. Naito, and M. Okuda, Transient currents in nematic liquid crystals, Phys. Rev. B **43**, 8272 (1991).

[18] H. Naito, M. Okuda, and A. Sugimura, Transient discharging processes in nematic liquid crystals, Phys. Rev. A **44**, R3434 (1991).

[19] H. Naito, K. Yoshida, and M. Okuda, Transient charging current in nematic liquid crystals, J. Appl. Phys. **73**, 1119 (1993).

[20] C. Colpaert, B. Maximus, and A. De Meyere, Adequate measuring techniques for ions in liquid crystal layers, Liq. Cryst. **21**, 133 (1996).

[21] A. Sawada, A. Manabe, and S. Nameura, A comparative study on the attributes of ions in nematic and isotropic phases, Jpn. J. Appl. Phys. **40**, 220 (2001).

[22] Y. Garbovskiy and I. Glushchenko, Nano-objects and ions in liquid crystals: Ion trapping effect and related phenomena, cryst. **5**, 501 (2015).

[23] S. Kumar, *Liquid Crystals: Experimental Studies of Physical Properties and Phase Transitions* (Cambridge University Press, Cambridge, UK, 2000).

[24] P. Keller and L. Liebert, Liquid crystal synthesis for physicists, in *Liquid Crystals*, Supplement 14, edited by L. Liebert (Academic Press, New York, 1978), pp. 20–75.

[25] J. L. Haberfeld, E. C. Hsu, and J. F. Johnson, Liquid crystal purification by zone refining, Mol. Cryst. Liquid Cryst. **24**, 1 (1973).

[26] F. Gaspard, R. Herino, and F. Mondon, Low field conduction of nematic liquid crystals studied by means of electrodialysis, Mol. Cryst. Liquid Cryst. **24**, 145 (1973).

[27] Y. Garbovskiy and I. Glushchenko, Ion trapping by means of ferroelectric nanoparticles, and the quantification of this process in liquid crystals, Appl. Phys. Lett. **107**, 041106 (2015).

[28] R. Basu and A. Garvey, Effects of ferroelectric nanoparticles on ion transport in a liquid crystal, Appl. Phys. Lett. **105**, 151905 (2014).

[29] Y.-S. Ha, H.-J. Kim, H.-G. Park, and D.-S. Seo, Enhancement of electro-optic properties in liquid crystal devices via titanium nanoparticle doping, Opt. Express **20**, 6448 (2012).

[30] C.-W. Lee and W.-P. Shih, Quantification of ion trapping effect of carbon nanomaterials in liquid crystals, Mater. Lett. **64**, 466 (2010).

[31] H. Y. Chen, W. Lee, and N. A. Clark, Faster electro-optical response characteristics of a carbon-nanotube-nematic suspension, Appl. Phys. Lett. **90**, 033510 (2007).

[32] R. Basu, Effect of carbon nanotubes on the field-induced nematic switching, Appl. Phys. Lett. **103**, 241906 (2013).

[33] R. Basu, Effects of graphene on electro-optic switching and spontaneous polarization of a ferroelectric liquid crystal, Appl. Phys. Lett. **105**, 112905 (2014).

[34] R. Basu, A. Garvey, and D. Kinnamon, Effects of graphene on electro-optic response and ion-transport in a nematic liquid crystal, J. Appl. Phys. **117**, 074301 (2015).

[35] P.-W. Wu and W. Lee, Phase and dielectric behaviors of a polymorphic liquid crystal doped with graphene nanoplatelets, Appl. Phys. Lett. **102**, 162904 (2013).

[36] P.-C. Wu, L. N. Lisetski, and W. Lee, Suppressed ionic effect and low-frequency texture transitions in a cholesteric liquid crystal doped with graphene nanoplatelets, Opt. Express **23**, 11195 (2015).

[37] D. P. Singh, S. K. Gupta, T. Vimal, and R. Manohar, Dielectric, electro-optical, and photoluminescence characteristics of ferroelectric liquid crystals on a graphene-coated indium tin oxide substrate, Phys. Rev. E **90**, 022501 (2014).

[38] W. Lee, C.-Y. Wang, and Y.-C. Shih, Effects of carbon nanosolids on the electro-optical properties of a twisted nematic liquid-crystal host, Appl. Phys. Lett. **85**, 513 (2004).

[39] R. K. Shukla, K. K. Raina, and W. Haase, Fast switching response and dielectric behavior of fullerene/ferroelectric liquid crystal nanocolloids, Liq. Cryst. **41**, 1726 (2014).

[40] R. Basu and A. Lee, Ion trapping by the graphene electrode in a graphene-ITO hybrid liquid crystal cell, Appl. Phys. Lett. **111**, 161905 (2017).

[41] R. Basu and L. Atwood, Reduced ionic effect and accelerated electro-optic response in a 2D hexagonal boron nitride planar-alignment agent based liquid crystal device, Opt. Mater. Express **9**, 1441 (2019).

[42] Y. Garbovskiy, Kinetics of ion-capturing/ion-releasing processes in liquid crystal devices utilizing contaminated nanoparticles and alignment films, Nanomaterials **8**, 59 (2018).

[43] C. Kohout, C. Santi, and L. Polito, Anisotropic gold nanoparticles in biomedical applications, Int. J. Mol. Sci. **19**, 3385 (2018).

[44] D. M. Samhadaneh, S. Chu, D. Maysinger, and U. Stochaj, How could gold nanourchins be applied in the clinic?, Nanomedicine **15**, 829 (2020).

[45] Z. Zou, N. A. Clark, and M. A. Handschy, Ionic transport effects in SSFLC cells, Ferroelectrics **121**, 147 (1991).

[46] P. G. De Gennes and J. Prost, *The Physics of Liquid Crystals* (Oxford University Press, New York, 1994).

[47] M. Imai, H. Naito, M. Okuda, M. Okuda, and A. Sugimura, Determination of rotational viscosity of nematic liquid crystals from transient current numerical analysis and experiment, Jpn. J. Appl. Phys., Part 1 **33**, 3482 (1994).

[48] M. Imai, H. Naito, M. Okuda, and A. Sugimura, Determination of rotational viscosity and pretilt angle in nematic liquid crystals from transient current influence of ionic conduction, Mol. Cryst. Liq. Cryst. Sci. Technol., Sect. A **259**, 37 (1995).

[49] M. Imai, H. Naito, M. Okuda, and A. Sugimura, A method for determination of rotational viscosity and pretilt angle from transient current in twisted nematic liquid crystal cells, Jpn. J. Appl. Phys., Part 1 **34**, 3170 (1995).

[50] A. Rastogi, F. Pandey, R. Manohar, and S. Singh, Effect of doping of $Cd_{1-x}Zn_xS/ZnS$ core/shell quantum dots in negative dielectric anisotropy nematic liquid crystal p-methoxybenzylidene p-decylaniline, cryst. **11**, 605 (2021).

[51] R. Basu, L. Atwood, and G. Sterling, Dielectric and electro-optic effects in a nematic liquid crystal doped with h-BN flakes, cryst. **10**, 123 (2020).

[52] D. Demus, J. Goodby, G. W. Gary, H.-W. Spiess, and V. Vill, *Physical Properties of Liquid Crystals* (Wiley VCH, Weinheim, Germany, 1999).

[53] G. Yadav, R. Katiyar, G. Pathak, and R. Manohar, Effect of ion trapping behavior of TiO_2 nanoparticles on different parameters of weakly polar nematic liquid crystal, J. Theor. Appl. Phys. **12**, 191 (2018).

[54] L. M. Blinov and V. G. Chigrinov, *Electro-optic Effects in Liquid Crystal Materials* (Springer-Verlag, New York, 1996).